

N82-232 72

0

**SDTIC**  
**ELECTE**  
JAN 25 1995  
**C D**

19951228 066

DEPARTMENT OF DEFENSE  
Approved for public release;  
Distribution Unlimited

THE FAILURE OF GLASS-REINFORCED COMPOSITES  
UNDER DYNAMIC TORSIONAL LOADING

T. Parry and J. Harding

O.U.E.L. Report. No. 1365/81

DEPARTMENT OF DEFENSE  
PLASTICS TECHNICAL EVALUATION CENTER  
WARRADCOM, WORMEY, N. C. 27591

REPRODUCED BY  
NATIONAL TECHNICAL  
INFORMATION SERVICE  
U.S. DEPARTMENT OF COMMERCE  
SPRINGFIELD, VA. 22161

PLASTEC  
143591

DTIC QUALITY INSPECTED 2

# DISCLAIMER NOTICE



**THIS DOCUMENT IS BEST QUALITY AVAILABLE. THE COPY FURNISHED TO DTIC CONTAINED A SIGNIFICANT NUMBER OF PAGES WHICH DO NOT REPRODUCE LEGIBLY.**

Date: 7/15/95 Time: 6:14:32PM

Page: 1 Document Name: untitled

1 OF 1  
---  
--- 1 - AD NUMBER: D436135  
--- 5 - CORPORATE AUTHOR: OXFORD UNIV (ENGLAND) DEPT OF ENGINEERING  
--- SCIENCE  
--- 6 - UNCLASSIFIED TITLE: THE FAILURE OF GLASS-REINFORCED COMPOSITES  
--- UNDER DYNAMIC TORSIONAL LOADING.  
---10 - PERSONAL AUTHORS: PARRY, T. ; HARDING, J. ;  
---11 - REPORT DATE: , 1981  
---12 - PAGINATION: 19P  
---14 - REPORT NUMBER: OUEL-1365/81  
---20 - REPORT CLASSIFICATION: UNCLASSIFIED  
---21 - SUPPLEMENTARY NOTE: IN: PROCEEDINGS OF THE COLLOQUE  
--- INTERNATIONAL DU CNRS NO. 319, 'PLASTIC BEHAVIOUR OF SOLIDS', 15-19  
--- JUN 81, VILLARD-DE-LANS.  
---22 - LIMITATIONS (ALPHA): APPROVED FOR PUBLIC RELEASE; DISTRIBUTION  
--- UNLIMITED. AVAILABILITY: NATIONAL TECHNICAL INFORMATION SERVICE,  
--- SPRINGFIELD VA. 22161. N82-23272.  
---33 - LIMITATION CODES: 1 24

--- END Y FOR NEXT ACCESSION

The failure of glass-reinforced composites under dynamic torsional loading

T. Parry\* and J. Harding

Department of Engineering Science, University of Oxford

(To appear in the Proceedings of the Colloque International du CNRS No. 319, 'Plastic Behaviour of Anisotropic Solids', Villard-de-Lans, June 15-19, 1981).

SYNOPSIS

Techniques for the impact testing of composite materials are briefly discussed. The application of the torsional Hopkinson pressure bar to the study of the dynamic failure of glass-reinforced epoxy-based composites is then described. Torque-twist curves are presented for thin-walled tubular specimens of cross-ply and woven mat reinforced laminates, cut with the specimen axis perpendicular to the interlaminar plane, at nominal average shear strain rates in the range 100 to 600 /s. The fracture surfaces are examined and a failure process is proposed, characterised by two stages, the initiation of failure by the formation of cracks on planes inclined at  $45^{\circ}$  to the specimen axis at a stress level strongly dependent on strain rate and the propagation of failure predominantly on interlaminar planes at a higher stress less strongly dependent on strain rate.

\* Now with Press Papers Ltd., 14 Stanhope Gate, London W1.

Accession For	
NTIS GRA&I	<input checked="" type="checkbox"/>
DTIC TAB	<input type="checkbox"/>
Unannounced	<input type="checkbox"/>
Justification	
By	
Distribution/	
Availability Codes	
Dist	Avail and/or Special
A-1	

## INDEX

	<u>Page</u>
1. <u>Introduction</u>	1
2. <u>Experimental Details</u>	2
2.1 Specimens	2
2.2 Test Procedure	3
3. <u>Results</u>	6
3.1 Mechanical Response	6
3.1.1 Oscilloscope stress-time records	6
3.1.2 Torque-Twist curves	6
3.1.3 Effect of strain rate on $\tau_y$	7
3.1.4 Effect of strain rate on $\tau_m$	8
3.2 Fracture Appearance	8
3.2.1 Cross-ply reinforced composite (XP/ER)	8
3.2.2 Woven glass reinforced composites	8
4. <u>Discussion</u>	9
5. <u>Conclusions</u>	11
<u>References</u>	12

## 1 Introduction

-/-

Much of the work that has been done on the impact response of composite materials has used the beam-type impact bending test [2]. Although this has for long been accepted as a standard test the very complex stress state involved makes it difficult to interpret the results obtained in any tolerably satisfactory way. The need has therefore been clear for some time for the development of simple impact tests in uniaxial tension, compression and pure shear [1].

Probably the most widely accepted technique for the impact testing of metallic materials is that using the split Hopkinson's pressure bar. Recently attempts have been made to adapt this technique to the testing of composite materials. The principal problems arise in connection with specimen design. The Hopkinson bar technique requires both that specimen dimensions should be small, so that wave propagation effects within the specimen may be ignored, and that the impedance mismatch between the specimen gripping system and the loading bars should be minimised to facilitate stress wave transmission at the interface with the specimen and to eliminate unwanted reflections.

These problems were largely avoided in an investigation using a punch-loading version of the Hopkinson bar apparatus [4] in which circular holes were punched in flat plates of woven-roving glass-reinforced laminates at punch speeds from  $2.5 \times 10^{-7}$  to 25 m/s. Although primarily a technological test in which only punch load-displacement curves could be obtained the results showed a very marked increase in the through-thickness shear strength, by some 250%, over the wide range of loading rates covered. The problem of the specimen gripping system is also simplified in the compression version of the Hopkinson bar apparatus, where short cylindrical specimens are used. Although this is not a standard design of compression specimen for composites testing, several attempts have been made to apply this technique to such materials [3, 5] and significant effects of strain rate have been observed.

Very recently Kawata et al. [7] have reported the successful development of a simple tensile impact test for composite materials in which cylindrical

specimens are used and the tensile load is applied through a screw fixing. The machine operates on the bar-block principle. Concurrently a modified version of the tensile Hopkinson bar has been developed at Oxford [13] using the more usual type of flat-plate specimen with parallel-sided grips. Even here, however, the constraints of the Hopkinson bar technique prevent a specimen of standard dimensions from being used. Consequently, when testing composite materials in both the compression and tensile versions of the Hopkinson bar, some uncertainty remains regarding the effect of using non-standard specimens on the severity of the stress concentrations at the specimen/loading bar interface.

This problem is much less severe, however, when the torsional version of the Hopkinson bar is used to test thin-walled tubular specimens in pure shear. In the past this technique has been applied most successfully to a wide range of ductile metallic materials [12]. Relatively recently it has also been applied to the testing of more brittle non-metallic materials including rocks [10] and oil shale and coal [6]. In the present paper its application to the testing of glass-reinforced epoxy composites is investigated. Torque-twist curves are obtained at nominal average shear strain rates from 100 to 600 s<sup>-1</sup>, the fracture surfaces are examined and the observed response discussed.

## 2 Experimental Details

### 2.1 Specimens

Tests have been performed on three commercially-available epoxy-based laminates, two (WR/ER and WR/7E) with a woven-roving glass mat reinforcement of closely similar geometry and, for comparison, one (XP/ER) with a non-woven cross-ply glass reinforcement. The WR/ER and XP/ER materials were supplied in the form of 12.5 mm thick laminated plate by Permali Ltd. of Gloucester. The WR/7E material was supplied in similar form by Stroud Insulations Ltd. of Preston. In each case the resin system was based on Araldite MY750 and Hardener HT976. Sections through the WR/ER and XP/ER plates on a plane perpendicular to one of the reinforcement directions are shown in figs. 1a and

lb respectively. The reinforcement geometries of the two woven composites are compared in Table I in terms of the average spacing between adjacent mats,  $c$ , the average wavelength,  $\lambda$ , and amplitude,  $a$ , of the weave and the glass/resin volume fraction,  $V_f$ . For the XP/ER material the average width of the individual laminae was 0.75 mm and the volume fraction was  $\sim 0.40$ .

Table 1 Reinforcement Geometry for Woven Composites

	$c$ (mm)	$\lambda$ (mm)	$a$ (mm)	$V_f$ (%)
WR/ER	0.208	2.117	0.049	0.40
XP/ER	0.192	1.588	0.055	0.41

The design of test specimen, see fig. 2 and Table II, follows that used in earlier work [11]. Here the specimen axis is perpendicular to the inter-laminar plane. The dimensions of the flanges,  $D$  and  $d$ , were chosen to give the same acoustic impedance as the loading bars to which they were attached, so as to minimise any unwanted wave reflections at these interfaces. The shorter gauge length (type II) specimens were required to allow the attainment of the highest strain rates. Only two individual laminae of XP material, and from 7 to 8 of WR material, were contained within the gauge length of the type II specimens, compared with 3 and 12 to 13, respectively in the type I specimens. Previous work on rocks [11] has shown specimen dimensions to have an effect on the failure process. The use of two different gauge lengths in the present tests allows a qualitative check for a similar effect in composite materials.

## 2.2 Test Procedure

A schematic view of the torsional Hopkinson bar apparatus and associated instrumentation and the corresponding Lagrangian wave propagation diagram are shown in figs. 3a and b respectively. The testing technique has been fully described elsewhere [8] so only a brief explanation will be given here. The specimen is attached to the input and output bars with araldite epoxy cement. To perform a test the input bar is clamped near its centre and an elastic torque,  $T$ , stored between the clamp and the rotating head. To

initiate the test the clamp is suddenly released, by the brittle fracture of a high strength steel bolt, causing an unloading wave, of magnitude  $T_1 = -T/2$ , to travel towards the rotating head, and a loading wave,  $T_1$ , to travel towards the specimen. At the specimen the loading wave is partially reflected and partially transmitted. Strain gauges attached to the input and output bars on either side of the specimen, stations I and II in fig. 3a, record the incident, reflected and transmitted waves and from these the torque applied to and the twist sustained by the specimen may be calculated, as in the standard compression version of the Hopkinson bar. However, the absence of end effects and of radial inertia in the torsional version of the apparatus allows very short gauge lengths to be used so that stress equilibrium across the specimen is achieved in times of less than 10  $\mu$ s [10], i.e. before the initial change in slope is reached on the resulting torque-twist curve. A typical set of strain gauge records, as displayed on an oscilloscope screen, for a test on a WR/ER specimen, is presented in fig. 4. Calibration lines are recorded on a separate photograph immediately before the test. The upper trace shows the incident loading wave, of magnitude  $T_1$ , and its subsequent unloading by the reflected wave, and the lower trace shows the torque  $T_2$  transmitted through the specimen. The relative angular velocity between the ends of the specimen is then given by

$$\dot{\theta}(t) = (2/J\rho c)(T_1 - T_2) \quad (1)$$

and the corresponding angular twist of the specimen by

$$\theta(t) = \int_0^t \dot{\theta} dt \quad (2)$$

On the assumption that the shear strain is uniform along the specimen gauge length, the average shear strain and shear strain rate may be obtained from

$$\gamma(t) = (r_m/l)\theta(t) \quad \text{and} \quad \dot{\gamma}(t) = (r_m/l)\dot{\theta}(t) \quad (3,4)$$

Treating the specimen as a series of parallel discs, this assumption is, perhaps, not unreasonable for the XP/ER material where successive discs are

nominally identical but for the  $90^\circ$  relative orientation. For the woven material, however, where the discs are, in this idealisation, alternately of unreinforced resin and woven glass mat, the shear strain in the resin is likely to exceed that in the reinforcement so that, in the limit, the matrix shear strain and strain rate may exceed the average values given by (3) and (4) by as much as a factor of  $(1/V_f)$ .

Assuming that the specimen deforms in pure shear and that stress equilibrium applies over the length of the specimen, the average shear stress is given by

$$\tau = T_2 / (2\pi r_m^2 h) \quad (5)$$

The early attainment of stress equilibrium has already been noted. The idealisation of the specimen into a series of parallel discs would imply that each supports the same applied shear stress so that no axial component of stress should be generated. To check whether this was indeed the case several tests were performed using, in addition, the axial strain gauges, station III in fig. 3a, to detect the presence of any axial wave propagating from the specimen. Strain gauge signals for transmitted torque (upper trace) and compressive axial force (lower trace) in tests on XP/ER material at a low rate,  $\dot{\gamma} \approx 50 \text{ s}^{-1}$ , and a high rate,  $\dot{\gamma} \approx 890 \text{ s}^{-1}$ , are shown in figs. 5a and b respectively. No axial force was detected in the low rate test but at the highest rates, where type II specimens were used, a significant axial force is developed. A similar behaviour was shown in tests on the woven material. In recording the shear and axial stress traces of figs. 5a and b, the shear trace was delayed in time to allow for the different wave speeds and strain gauge positions so that, as displayed on the oscilloscope screen, both traces have the same time zero. It is then clear, see fig. 5b, that a significant axial force is not generated until after the maximum torque has been reached. Equation (5) may, therefore, be taken as valid up to this point in the test.

### 3 Results

#### 3.1 Mechanical Response

##### 3.1.1 Oscilloscope stress-time records

It is clear from the transmitted stress-time trace of fig. 4 that the specimen behaviour may be characterised by an initial linear response up to an 'elastic limit' torque,  $T_y$ , corresponding to a shear stress  $\tau_y$ , followed by a slower, non-linear, increase of torque with time until a limiting torque,  $T_m$ , corresponding to an ultimate shear stress  $\tau_m$ , is reached. Beyond the peak torque specimens of the XP material show a very rapid decline in the torque supported by the specimen, see figs. 5a and b, whereas in woven reinforced specimens the torque decreases more slowly at first and subsequently at a more rapid rate, see fig. 5c. In neither case, however, is the specimen completely unloaded, a small residual torque remaining throughout the period covered by the oscilloscope traces, i.e. for more than 500  $\mu$ s.

In tests on type II specimens of both XP/ER and WR/ER materials one or two oscillations were observed on the oscilloscope transmitted torque trace in the region between  $T_y$  and  $T_m$ , see fig. 5d. Since type II specimens were used, in the main, at the highest strain rates, it was not clear whether this effect was due to the change in gauge length or whether it reflected a material response to increasing strain rate. For WR/ER material, however, comparison tests were performed at an intermediate strain rate on specimens of both types and the resulting oscilloscope traces both showed a few very small amplitude oscillations immediately following  $T_y$ . This suggests that the effect is not related to the difference in specimen gauge length but represents an increasing instability in the deformation process immediately following  $T_y$  with increasing strain rate.

##### 3.1.2 Torque-Twist Curves

Torque-twist curves for the test of fig. 4 and for a similar test at a higher rate are shown in fig. 6, using equations (1) and (2) to calculate the angle of twist. The variation of nominal shear strain rate during each

test, calculated from equation (4) assuming uniform strain along the gauge length, is also shown in fig. 6. The strain rate decreases during the test, by about a factor of 2 in the lower rate test and by rather less at the higher rate. Nevertheless, at any given angle of twist there is a large and nearly constant difference in torque between the two tests despite the relatively small difference in average nominal shear strain rate,  $\sim 150 \text{ s}^{-1}$  and  $\sim 500 \text{ s}^{-1}$  for the lower and upper curves respectively. Both curves are for tests on type I specimens. Similar torque-twist curves for type I specimens of XP material are shown in fig. 7 for tests at average strain rates of  $\sim 80 \text{ s}^{-1}$  and  $\sim 240 \text{ s}^{-1}$ . Again a marked effect of strain rate is observed. For the XP/ER specimens, however, the torque at a given angle of twist is significantly greater than for WR/ER specimens at the same strain rate, although the angle of twist at failure, i.e. at  $T_m$ , is very much less.

### 3.1.3 Effect of strain rate on $\tau_y$

In most tests the elastic limit torque,  $T_y$ , can be determined, relatively unambiguously, from the relevant oscilloscope transmitted torque trace or the corresponding torque-twist curve. The variation of the equivalent shear yield stress,  $\tau_y$ , determined using equation (5), with the logarithm of the instantaneous nominal strain rate at this point in each test, is shown in fig. 8. Each data point relates to an individual test. Two distinct curves, shown dashed in fig. 8, are obtained, one for XP material, the other for the two woven composites. Both curves fit an empirical relationship of the form  $\tau_y = K\dot{\gamma}_y^n$  where the values of the constants K and n are 0.9 MPa and 0.65, respectively, for XP/ER and 0.16 MPa and 0.83 for the woven materials. In both cases the results for the type II specimens appear to lie on an extrapolation to higher strain rates of the curve for type I specimens, suggesting that, within the small range studied,  $\tau_y$  is independent of specimen gauge length. This conclusion was supported, for WR/ER specimens, by the deliberate inclusion of a test on a type II specimen at a lower strain rate, giving a value of  $\tau_y$  close to that for type I specimens at the same strain rate.

#### 3.1.4 Effect of strain rate on $\tau_m$

A similar plot of the variation of the ultimate shear stress,  $\tau_m$ , obtained from  $T_m$  using equation (5), with the logarithm of the instantaneous nominal strain rate at this point in the test is shown in fig. 9. Again each data point represents an individual test. Here the behaviour is rather different from that shown in fig. 8. The results for the two woven composites fall on two clearly distinct curves. The ultimate shear stress for the WR/ER composite lies significantly above that for the XP material. Whereas, within the limits of experimental scatter,  $\tau_m$  appears to be independent of specimen gauge length for the XP material, results for the type II WR/ER specimens lie significantly below those for the type I specimens. For all three composites the rate dependence of  $\tau_m$  is markedly less than that of  $\tau_y$ .

### 3.2 Fracture Appearance

#### 3.2.1 Cross-ply reinforced composite (XP/ER)

Two views of the fracture surface, one parallel, the other perpendicular, to the axis of an XP/ER specimen which had been tested at  $\sim 100 \text{ s}^{-1}$  are shown in fig. 10. It is clear that fracture, in general, follows the interlaminar plane, i.e. the plane supporting the maximum shear stress, with occasional jumps between adjacent interlaminar planes on steps inclined at  $\sim 45^\circ$  to the specimen axis, points A in fig. 10. These steps are on planes parallel to the reinforcement direction in that part of the specimen they are crossing and are usually found close to regions where the reinforcement lies in a radial direction, i.e. on planes across which the maximum tensile stress is developed. As a result, in the specimen shown in fig. 10 the fracture surface traverses three individual laminae while propagating around the circumference of the specimen. For complete separation of the two parts of the specimen the fracture surface has to traverse back across these three laminae. This it does at point B in fig. 10, on three mutually perpendicular  $45^\circ$  planes.

#### 3.2.2 Woven-glass reinforced composites

Two views of the fracture surface of a WR/ER specimen, again observed

9

parallel to and perpendicular to the specimen axis, are shown in fig. 11 for a specimen tested at a rate of  $\approx 300 \text{ s}^{-1}$ . A relatively smooth spiral path is followed, principally on the interlaminar plane but crossing several layers of reinforcement while propagating around the circumference of the specimen and leading to a region of overlap some 7 to 8 laminae thick where the crack has propagated through more than  $360^\circ$ . Final separation of the two parts of the specimen is across this overlap region on a plane approximately parallel to the specimen axis.

Except in the resin only regions, the formation of tensile cracks on planes inclined at  $45^\circ$  to the axis and across the full wall thickness of the specimen will be inhibited by the bi-directional nature of the glass reinforcement. Nevertheless, small gaps are present between adjacent parallel rovings through which such cracks might propagate from one resin only region to the next. That in practice  $45^\circ$  cracks crossing several reinforcement layers could be obtained is shown in fig. 12a and is implied by the spiral nature of the fracture surface. Examination at high magnification of the crack in the overlap region, see fig. 12b, revealed that failure was predominantly at the resin/reinforcement interface but with frequent jumps across the resin from one interface to the next. The crack was also observed to pass between warp and weft rovings, at which points it often propagated into the next resin only region.

#### 4 Discussion

Insufficient data are available to allow an unambiguous description of the dynamic torsional failure process in the woven and cross-ply composites. It would seem not unreasonable, however, to associate  $T_y$  with the development of tensile cracking on  $45^\circ$  planes and  $T_m$  with the propagation of failure between such cracks on the interlaminar plane for XP material, or the observed spiral fracture surface, for woven material. Following  $T_m$ , in XP specimens the torque unloads very rapidly, reflecting the relatively smooth nature of the interlaminar fracture surface, whereas for WR specimens the torque decreases more slowly from a higher maximum, reflecting the greater energy absorbed

when fracture follows the woven glass/resin interface.<sup>10</sup>

This qualitative description of the fracture process presents several difficulties. Thus, the formation of cracks on  $45^\circ$  planes should lead to the development of compressive stresses on the adjacent region of the interlaminar plane equal in magnitude to the applied shear stress at torques greater than  $T_y$ . Unlike in earlier work on rocks [11], however, there was little evidence for the development of an axial stress until after  $T_m$  was reached. It may be argued that, whereas in the rock specimens the  $45^\circ$  cracks could extend over the entire gauge length and form at all points on the periphery, in tests on composites the cracks are inhibited from crossing the interlaminar plane and in the XP material are only likely to form in two regions of the periphery, thus limiting the resulting effective axial force. Nevertheless, cracking in the composite specimens has to be sufficiently extensive to account for the significant decrease in torsional stiffness beyond  $T_y$ .

An indication of the extent of such cracking in the woven composites is given in fig. 13. This shows part of the cracked region of fig. 12b at a higher magnification using interference contrast to reveal the reinforcing fibres, see fig. 13a, and direct reflected light to reveal the cracks, see fig. 13b. It is apparent that those cracks in the resin inclined to the interlaminar plane have opened up to a considerable extent and are accommodated by secondary cracks developed at, or parallel to, the resin/reinforcement interface. The region shown was part of a system of cracks which did not lie on the final fracture surface but nevertheless contributed to the relatively high overall strain at failure obtained in the WR/ER specimens where, at the highest rates,  $\gamma_m$  approached 8%. This compares with the cross-ply material where  $\gamma_m$  was both much lower,  $\sim 2\%$ , and independent of strain rate. The intermediate response of the WR/7E material, where  $\tau_m$  remains low, at about the same level as for XP specimens, and where  $\gamma_m \sim 4\%$  and is again independent of strain rate, may reflect different critical conditions at the resin/reinforcement interface resulting from slightly different conditions of manufacture.

Two other factors require to be discussed; the effect of gauge length

//

and of strain rate on  $\tau_y$  and  $\tau_m$ . If  $\tau_y$  represents a fracture initiation stress in a localised region of the specimen its independence of gauge length is not unexpected. In the cross-ply material steps on the final fracture surface are only found at certain positions on the periphery so the fracture path, and hence  $T_m$ , might again be expected to be independent of gauge length. In the woven material, however, the longer gauge length allows cracks to form initially at a greater separation along the axial direction making their subsequent coalescence more difficult, i.e. increasing  $T_m$ .

While the rate dependence of both  $\tau_y$  and  $\tau_m$  is likely to be a reflection of the behaviour of the epoxy resin, for which the flow strength is known to increase greatly with rate of strain [9], a direct correlation is not possible because of the influence of the reinforcement. Thus, since  $\tau_m$  is largely controlled by the ease of crack propagation at the resin/reinforcement interface or the interlaminar plane in woven and cross-ply specimens respectively, its small but significant rate dependence may be presumed to reflect the behaviour at these interfaces rather than in the resin alone. Equally, local stress concentrations related to the particular reinforcement/resin arrangement in a given region are likely to be important in determining the applied stress  $\tau_y$  at which fracture initiates. Nevertheless, if these local stress concentrations are not greatly affected by strain rate and if fracture initiation depends on the attainment of a critical strain in the resin, the marked rate dependence of  $\tau_y$  would follow from the much higher stresses associated with a given strain in the resin at the higher strain rates.

Although in large part this discussion has been highly speculative, the proposal that  $\tau_y$  represents the stress at which tensile cracks develop and  $\tau_m$  represents the propagation of failure predominantly on the interlaminar plane still appears the most likely interpretation of the observed torque-twist curves and fracture surfaces.

## 5 Conclusions

The torsional Hopkinson bar has been adapted to the testing of composite materials in shear on the interlaminar plane. Torque-twist curves have been

obtained at nominal average strain rates from 100 to 600 s<sup>-1</sup>. These are characterised by a yield torque, T<sub>y</sub>, which is strongly rate dependent, and a maximum, or failure, torque, T<sub>m</sub>, which is less rate dependent. A tentative description of the failure process relates T<sub>y</sub> to the initiation of tensile cracks on 45° planes and T<sub>m</sub> to their propagation on interlaminar planes.

#### References

1. Adams, D.F. "Impact response of polymer-matrix composite materials." ASTM STP 617, American Society for Testing Materials, (1977): 409-426.
2. Adams, D.F. and A.K. Miller. "An analysis of the impact behaviour of hybrid composite materials." Materials Science and Engineering 19 (1975): 245-260.
3. Griffiths, L.J. and D.J. Martin. "A study of the dynamic behaviour of a carbon-fibre composite using the split Hopkinson pressure bar." J. Phys. D: Appl. Phys. 7 (1974): 2329-2341.
4. Harding, J. "The high-speed punching of woven-roving glass-reinforced composites." in Mechanical Properties at High Rates of Strain Inst. Phys. Conf. Ser. No. 47, (1979): 318-330.
5. Huddart, J. "The compressive strength of fibre-reinforced plastics." Ph.D. Thesis, Imperial College, University of London (1975).
6. Jahsman, W.E. "Dynamic fracture strength of oil shale and coal." Oxford University Engineering Laboratory Report No. 1295/79 (1979): 1-26.
7. Kawata, K., A. Hondo, S. Hashimoto, N. Takeda and H.L. Chung. "Dynamic behaviour analysis of composite materials." in Composite Materials Proc. Japan - U.S. Conference, Tokyo (1981): 2-11.
8. Lewis, J.L. and J.D. Campbell. "The development and use of a torsional Hopkinson-bar apparatus." Experimental Mechanics 12 (1972): 520-524
9. Lindholm, U.S. "Some experiments with the split Hopkinson pressure bar." J. Mech. Phys. Solids 12 (1964): 317-335.
10. Lipkin, J., D.E. Grady and J.D. Campbell. "Dynamic flow and fracture of rock in pure shear." Proc. 18th U.S. Symposium on Rock Mechanics 3B2 (1977): 1-7.
11. Lipkin, J., K.W. Schuler and T. Parry. "Dynamic torsional failure of limestone tubes." in Mechanical Properties at High Rates of Strain Inst. Phys. Conf. Ser. No. 47, (1979): 101-110.
12. Tsao, M.C.C. and J.D. Campbell. "Plastic shear properties of metals and alloys at high strain rates." Oxford University Engineering Laboratory Report No. 1055/73 (1973): 1-83.
13. Welsh, L.M. (unpublished work).



Fig. 1a Section through WR/ER material (x76)

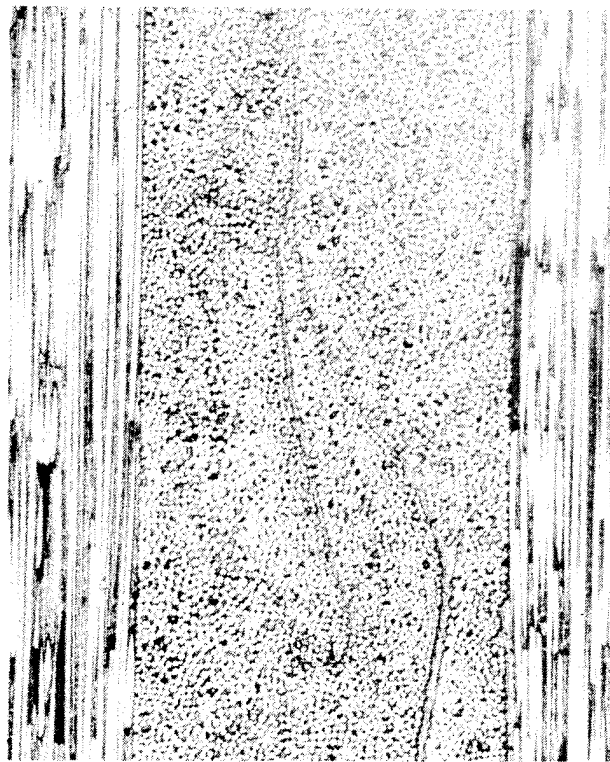


Fig. 1b Section through XP/ER material (x 68)

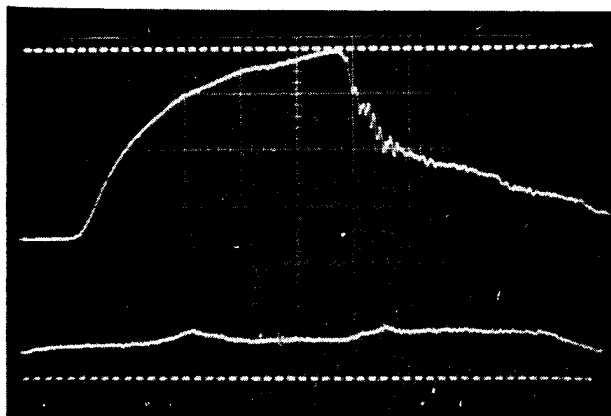


Fig. 5a Output torque and axial force traces for XP/ER specimen tested at a low rate ( $\dot{\gamma}_m \approx 50/s$ )

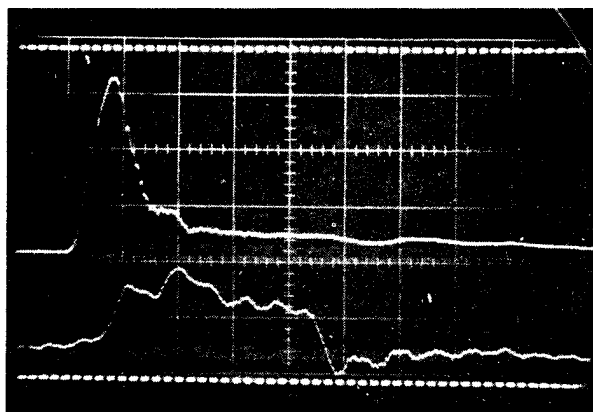


Fig. 5b Output torque and axial force traces for XP/ER specimen tested at a high rate ( $\dot{\gamma}_m \approx 890/s$ )

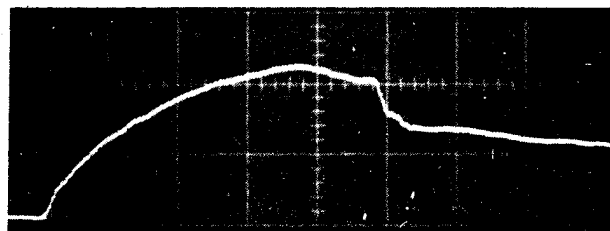


Fig. 5c Output torque trace for WR/ER specimen tested at a low rate ( $\dot{\gamma}_m \approx 50/s$ ) showing unloading region beyond  $T_m$

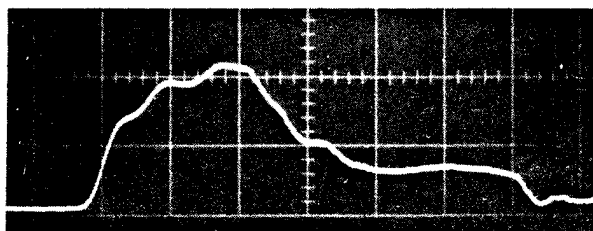


Fig. 5d Output torque trace for type II WR/ER specimen tested at a high rate ( $\dot{\gamma}_m \approx 1100/s$ ) showing oscillations following  $T_y$

Fig. 2 Specimen Design

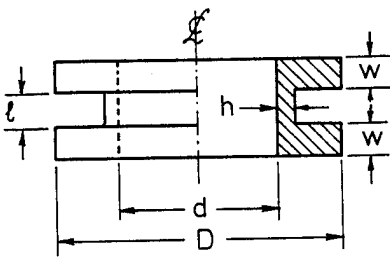


Table II Specimen Dimensions (mm) 14

		l	h	d	D	W
WR/ER and XP/ER	Type I	2.5	1.5	10	34.8	5.0
	Type II	1.5	1.5	15	35.0	5.0
WR/7E	Type I	2.5	1.5	10	34.8	3.5

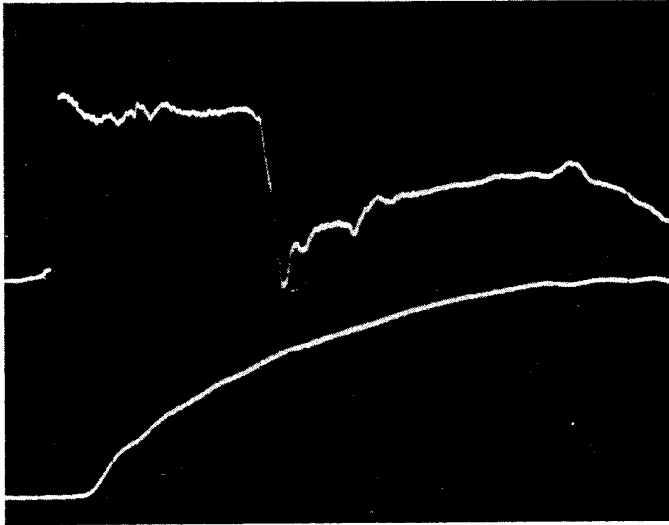


Fig. 4 Typical oscilloscope traces for a test on a WR/ER specimen

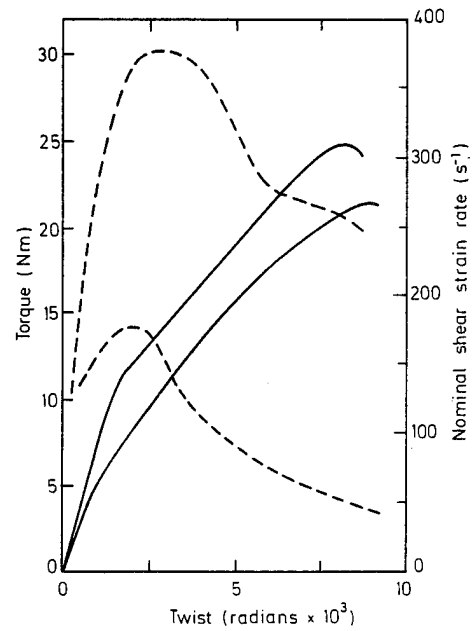


Fig. 7 Torque-twist curves for XP/ER specimens

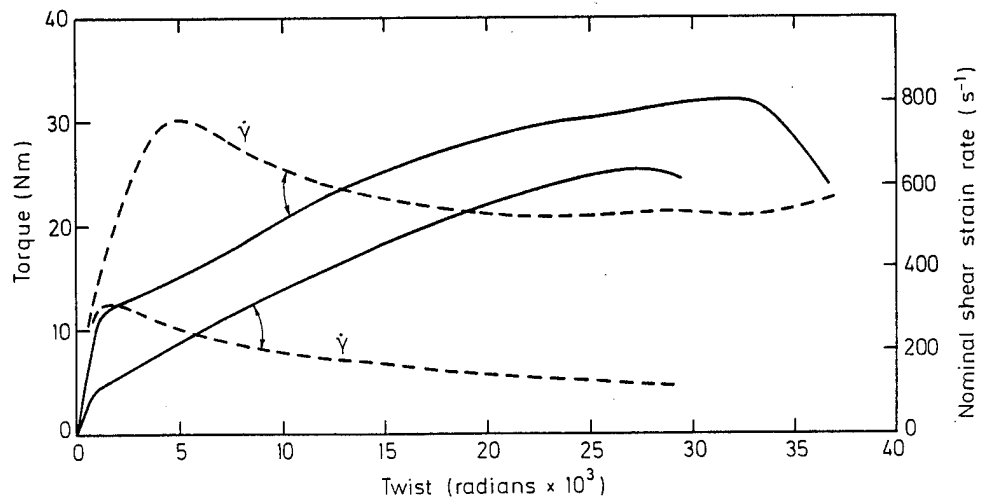


Fig. 6 Torque-twist curves for WR/ER specimens

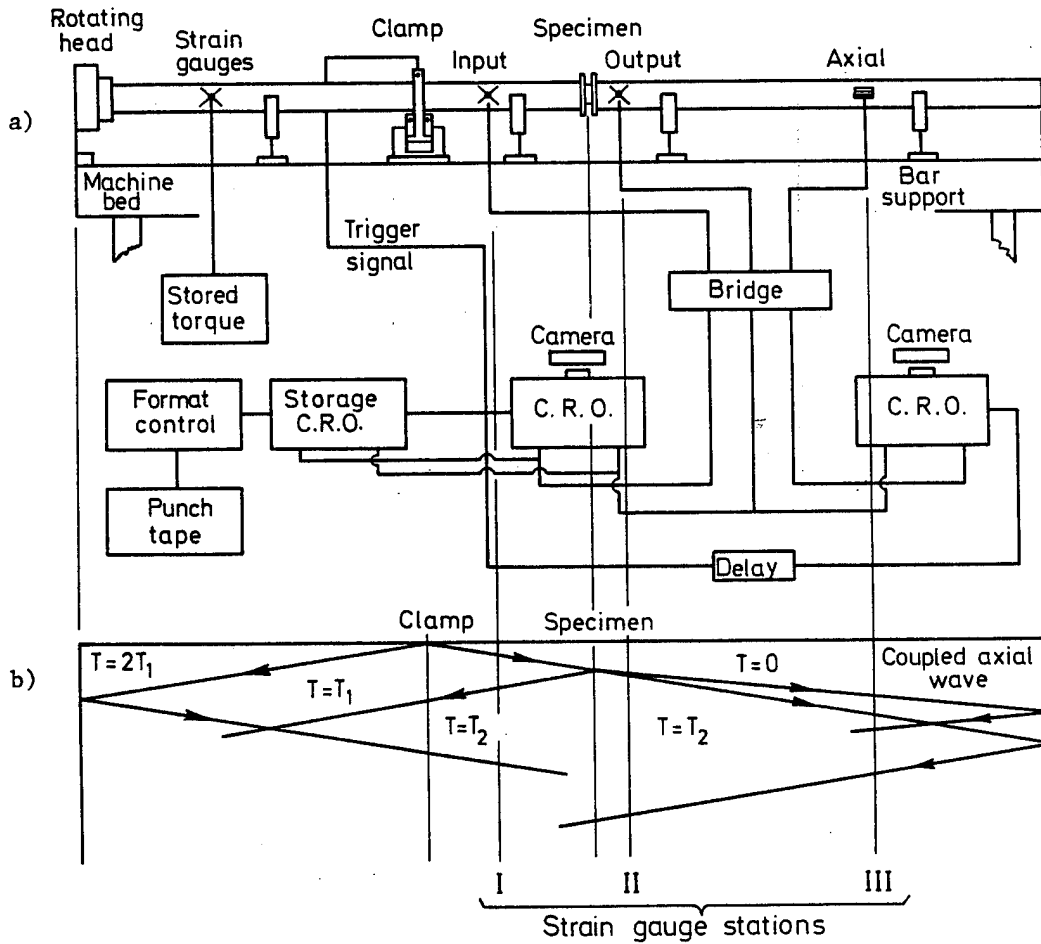


Fig. 3 a) Schematic view of torsional Hopkinson bar apparatus and associated instrumentation  
 b) Lagrangian wave propagation diagram for torsional Hopkinson bar

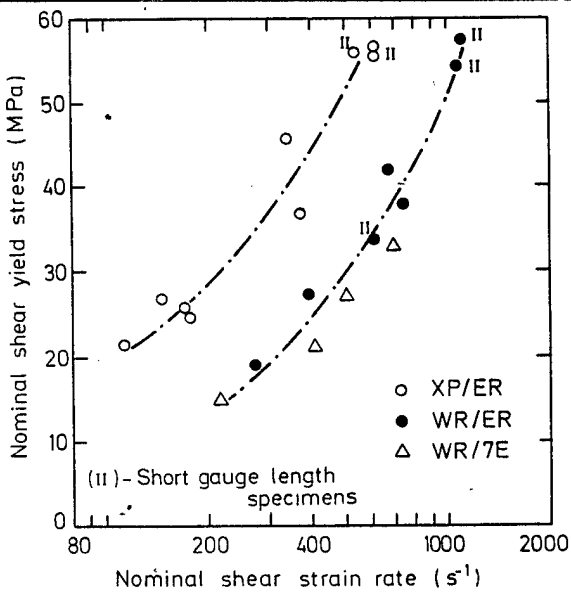


Fig. 8 Variation of  $\tau_y$  with strain rate at yield

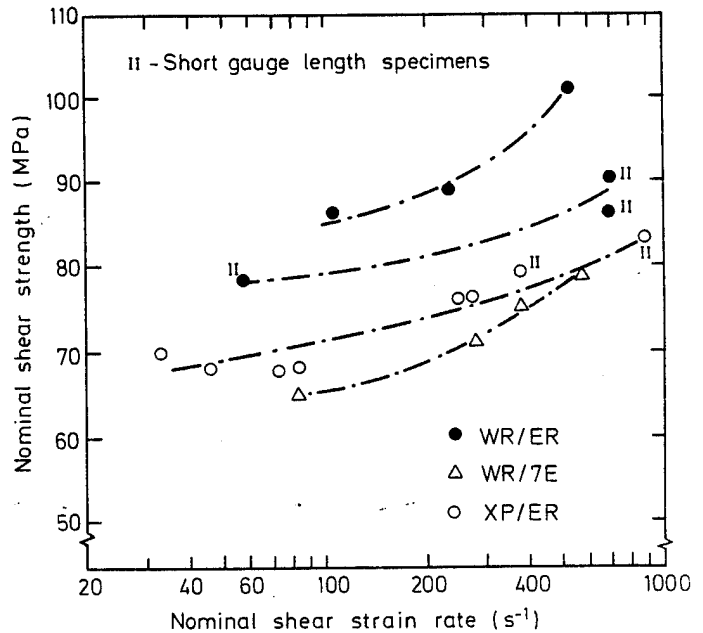


Fig. 9 Variation of  $\tau_m$  with strain rate at maximum torque

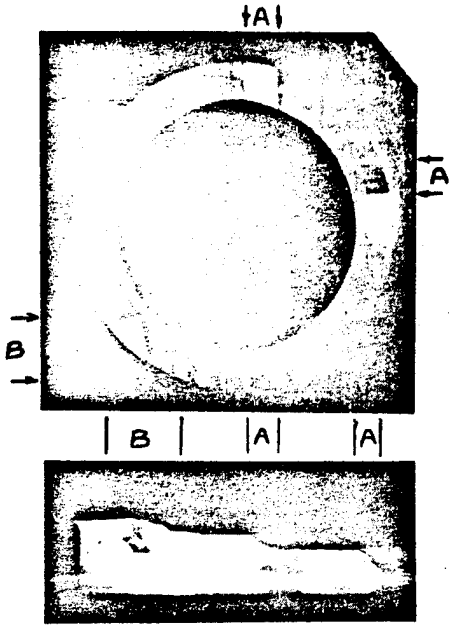
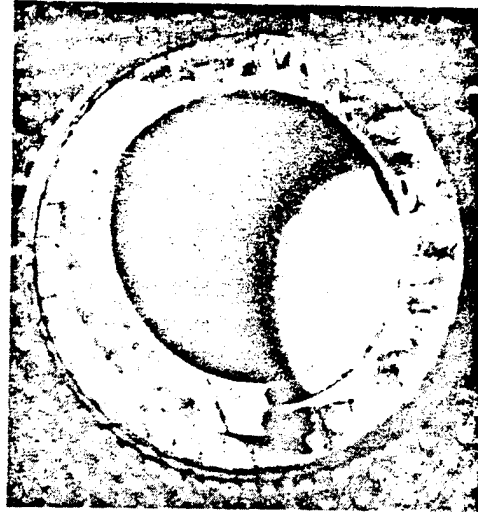


Fig. 10 Fracture surface of XP/ER specimen viewed a) perpendicular to and b) parallel to interlaminar plane (x4)  
 A - steps at 45° between adjacent interlaminar planes  
 B - steps at 45° across 3 adjacent laminae



b)



Fig. 11 Fracture surface of WR/ER specimen viewed a) perpendicular to and b) parallel to interlaminar plane showing spiral fracture surface and overlap region (x5)



Fig. 12a Tensile cracks on 45° planes in WR/ER specimen (x5)

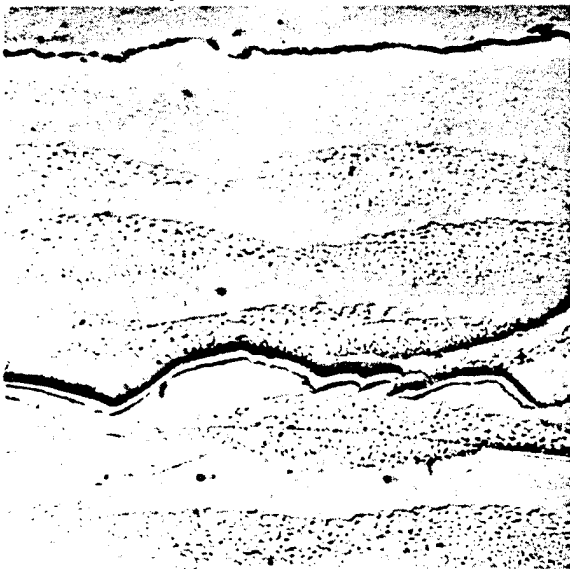
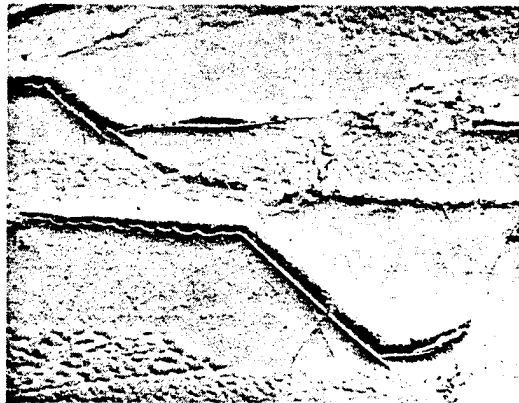


Fig. 12b Crack path in overlap region of Fig. 11 (x 52)

a)



b)

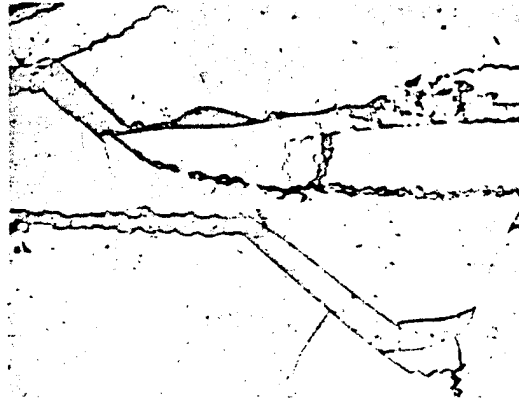


Fig. 13 Extensive cracking in overlap region of Fig. 11 using a) interference contrast to reveal reinforcement and b) direct illumination to reveal cracks (x 120)